JOURNAL OF AIRCRAFT
Vol. 37, No. 5, September–October 2000

Nonlinear Aeroelastic Analysis of Complete Aircraft in Subsonic Flow

Mayuresh J. Patil* and Dewey H. Hodges†
Georgia Institute of Technology, Atlanta, Georgia 30332
and
Carlos E. S. Cesnik‡
Massachusetts Institute of Technology, Cambridge, Massachusetts 02139

Aeroelastic instabilities are among the factors that may constrain the flight envelope of aircraft and, thus, must be considered during design. As future aircraft designs reduce weight and raise performance levels using directional material, thus leading to an increasingly flexible aircraft, there is a need for reliable analysis that models all of the important characteristics of the fluid–structure interaction problem. Such a model would be used in preliminary design and control synthesis. A theoretical basis has been established for a consistent analysis that takes into account 1) material anisotropy, 2) geometrical nonlinearities of the structure, 3) unsteady flow behavior, and 4) dynamic stall for the complete aircraft. Such a formulation for aeroelastic analysis of a complete aircraft in subsonic flow is described. Linear results are presented and validated for the Goland wing (Goland, M., "The Flutter of a Uniform Cantilever Wing," *Journal of Applied Mechanics*, Vol. 12, No. 4, 1945, pp. A197–A208). Further results have been obtained that highlight the effects of structural and aerodynamic nonlinearities on the trim solution, flutter speed, and amplitude of limit-cycle oscillations. These results give insight into various nonlinear aeroelastic phenomena of interest: 1) the effect of steady-state lift and accompanying deformation on the speed at which instabilities occur, 2) the effect on nonlinearities in limiting the amplitude of oscillations once an instability is encountered, and 3) the destabilizing effects of nonlinearities for finite disturbances at stable conditions.

Nomenclature

b = semichord
C^{ab} = direction cosine matrix from frame b to frame a
c_d = drag coefficient
D = drag per unit length
$\boldsymbol{e}_i$ = unit vector in the ith direction
F = internal force
f = external force (aerodynamic)
G = gravitational energy
H = linear momentum
h_n = generalized airfoil deformations
I = inertia matrix
K = kinetic energy
L_n = generalized lift distribution
$\mathcal{L}$ = wing length
M = internal moment
$\mathcal{M}$ = mass
m = external applied moment
P = angular momentum
$\boldsymbol{r}$ = position vector from aircraft reference point
$\mathcal{S}$ = stiffness matrix
U = potential energy
u_0 = aircraft forward velocity
V = linear velocity (structural)
v_n = generalized velocity perpendicular to airfoil
X = structural variables
Y = induced-flow variables
Γ = circulation
γ = strain
Δ = identity matrix
Δc_n = reduction in generalized loads due to stall (static)
δ = variational operator
$\overline{\delta\mathcal{A}}$ = virtual action
$\overline{\delta W}$ = virtual work
θ = Rodrigues parameters
κ = curvature
λ_n = induced-flow expansion coefficients
ξ = mass offset
ρ = density of air
Ω = angular velocity

Subscripts

b = wing reference point
f = fuselage properties
w = wing properties
0 = fuselage reference point

Superscripts

a = aircraft frame
B = deformed wing (beam) frame
b = wing (beam) undeformed frame
i = inertial frame
$\dot{(\,)}$ = derivative with respect to time
$(\,)'$ = derivative with respect to x_1
$\bar{(\,)}$ = steady-state solution
$\hat{(\,)}$ = small perturbation about steady state
$\tilde{(\,)}$ = dual matrix

Received 27 December 1998; revision received 28 February 2000; accepted for publication 10 April 2000. Published by the American Institute of Aeronautics and Astronautics, Inc., with permission.

*Graduate Research Assistant, School of Aerospace Engineering. Member AIAA.
†Professor, School of Aerospace Engineering. Fellow AIAA.
‡Assistant Professor, Aeronautics and Astronautics. Senior Member AIAA.

Introduction

THE last decade has seen an expansion of the flight envelope of aircraft as well as an increase in the variety of flight missions. Aeroelastic tailoring of composite wings opened an era in which structural coupling could be used favorably, making new concepts such as forward swept wings possible. High-aspect-ratio wings have come into prominence lately due to the interest in high-altitude

long-endurance (HALE) uninhabited aerial vehicles (UAVs) for future military as well as civilian missions. An increase in flight performance is desired and would have to be accompanied by very robust and intelligent controllers. Here flight maneuvers that were once discarded due to their uncertainties could be considered during design if the aircraft model (analysis) possesses all of the physical characteristics of the aircraft. Then stall could be a regular part of the flight trajectories, and control reversal could be used effectively as control augmentation. There is a need for a model that takes into account the higher-order, nonlinear effects and the various couplings.

An accurate modeling of nonlinear phenomena in aeroelasticity is bound to be an integral part of next generation aircraft design. Such a model would also be required in designing a control system for the entire expected flight regime. This paper presents the ongoing research toward development of such a model. High-fidelity computational techniques are already available for both the structural analysis and aerodynamics, but the emphasis in this research is on using a far less computationally expensive model. To accomplish that, the goals set for this work are 1) development of an inexpensive but reasonably high-fidelity model that might help get more insight into the true nonlinear aeroelastic behavior and 2) building an analysis tool useful in preliminary design and control system design.

There is a vast amount of literature available in the field of aeroelasticity. The development of theories for aeroelastic analyses, which started with simplistic models of linear modal analysis for structures and one-dimensional quasi-steady aerodynamics, have come a long way to the point that tools based on coupling the computational structural dynamics and computational fluid dynamics are in current use. An overview of recent and ongoing research in related fields is presented in detail in an earlier paper.[1]

Aeroelastic analysis of composite wings is a subject of an ever increasing body of literature. The interest stems from the possibility of using directional properties of composites to optimize a wing, that is, aeroelastic tailoring. Shirk et al.[2] presented a historical background of aeroelastic tailoring and the theory underlying the technology. Librescu and Song were among the first to use a more realistic cross section, a box beam model made up of various composite laminates for the wing,[3] as opposed to laminated plates. This type of model was analyzed for static aeroelastic instabilities. Butler and Banerjee,[4] Chattopadhyay et al.,[5] Cesnik et al.,[6] and Patil[7] have investigated the influence of ply-angle layup on the static and dynamic aeroelastic characteristics of composite box beams.

Aeroelastic characteristics of highly flexible aircraft is investigated by van Schoor and von Flotow.[8] The complete aircraft was modeled using a few modes of vibration, including rigid-body modes. Waszak and Schmidt[9] used Lagrange's equation to derive the nonlinear equations of motion for a flexible aircraft. Generalized aerodynamic forces are added as closed-form integrals. This form helps in identifying the effects of various parameters on the aircraft dynamics.

Nonlinear aeroelastic analysis has gathered a lot of momentum in the last decade due to understanding of nonlinear dynamics as applied to complex systems and the availability of the required mathematical tools. The studies conducted by Dunn and Dugundji are a combination of analysis and experimental validation of the effects of dynamic stall on aeroelastic instabilities for simple cantilevered laminated platelike wings.[10] Virgin and Dowell have looked into the nonlinear behavior of airfoils with control surface free play and investigated the limit-cycle oscillations and chaotic motion of airfoils.[11] On the other hand, nonlinear aeroelastic behavior of an airfoil supported by nonlinear springs was investigated by Gilliatt et al.[12]

The authors[1,6] have analyzed the nonlinear behavior of cantilevered box beams in subsonic flow. The studies include the structural nonlinearities arising due to large displacements and aerodynamic nonlinearities due to stall. Stall modeling is very important for HALE aircraft because the flight at high altitude (low density) and low speeds would necessitate a high trim angle of attack. Furthermore, because of the length of the wing and the accompanying elastic deformations, it is possible for the wing tip to encounter stall. Aeroelastic characteristics of the wing were analyzed from the standpoint of stability. The present paper describes the theory supporting the nonlinear aeroelastic behavior of a wing and investigates the effects of the various nonlinearities on the aeroelastic stability as well as high-amplitude response. As such, it is the first time that a geometrically exact structural model is coupled to a nonlinear aerodynamic model that includes dynamic stall effects. The results are, thus, relevant in understanding the nonlinear aeroelastic behavior of high-aspect-ratio wings and the need to include nonlinearities in the modeling process.

Formulation

The theory is based on two separate works, namely, 1) mixed variational formulation based on exact intrinsic equations for dynamics of moving beams[13] and 2) finite state airloads for deformable airfoils on fixed and rotating wings.[14,15] The former theory is a nonlinear intrinsic formulation for the dynamics of initially curved and twisted beams in a moving frame. There are no approximations to the geometry of the reference line of the deformed beam or to the orientation of the cross-sectional reference frame of the deformed beam. A compact mixed variational formulation can be derived from these equations, which is well-suited for low-order beam finite element analysis[16] based in part on the original paper by Hodges.[13] The latter work presents a state-space theory for the lift, drag, and all generalized forces of a deformable airfoil. Trailing-edge flap deflections are included implicitly as a special case of generalized deformation. The theory models a thin airfoil that can undergo arbitrary small local deformations with respect to a reference frame that can perform arbitrary large global motions.

Structural Theory

During the last nine years, a comprehensive framework has been developed for modeling of generally nonhomogeneous, anisotropic beams with arbitrary cross-sectional geometry and material distribution.[17,18] With the modeling power of the finite element method, it takes a two-step modeling approach, which facilitates the accurate treatment of complicated, built-up beamlike structures with a very small number of states. It is based on three-dimensional elasticity and is capable of modeling complex cross-sectional geometry (solid, built up, thick walled, or thin walled; open or closed; airfoil shaped if necessary), including all possible couplings and deformation in an asymptotically correct manner.

The framework of structural analysis also gives rise to a set of geometrically exact nonlinear equations for the beam structural dynamics.[13] Thus, it provides a concise and accurate formulation for handling built-up, beamlike structures undergoing large motions with geometrically nonlinear deformation. It has been successfully applied to rotary-wing static and dynamic aeroelastic stability problems[19] and aircraft composite-wing aeroelastic analysis.[1] This formulation is ideally suited for large motion and geometrically nonlinear deformation of wings structures and will be used here as the starting point.

The formulation presented is an extension of the mixed variational formulation for dynamics of moving beams. It includes global frame motion as variable, and is thus able to handle aircraft dynamics and gravitational potential. To generate the equations for this problem, the only changes are the inclusion of the appropriate energies in the original formulation. The equations of motion are obtained by application of the calculus of variations.

There are various reference frames used in the formulation: i is the inertial reference frame, with i_3 vertically upward (needed to define the direction of gravitational forces); a is a frame attached to the aircraft, with a_2 pointing toward the nose and a_3 pointing upward; b is a series of frames attached to the undeformed beam (wing) reference line, b_1 is along the reference line; B is the deformed beam reference frame. The superscripts i, a, b, and B refer to the frame in which a given vector is expressed.

Note that the formulation is presented here assuming just one wing for clarity. In actual implementation, a user-defined number of wings is allowed, thus accounting for two wings, tail wings, vertical stabilizer, canard, or any other winglike surfaces.

The variational formulation is derived from Hamilton's extended principle, which can be written as

$$\int_{t_1}^{t_2} [\delta(K - U) + \overline{\delta W}]\,\mathrm{d}t = \overline{\delta \mathcal{A}} \tag{1}$$

where t_1 and t_2 specify the beginning and end, respectively, of the time interval over which the solution is required.

The kinetic energy of the system comes from the two subsystems that have mass, namely, fuselage and wing. The kinetic energies for the fuselage (modeled as a rigid body) and the wing (modeled as a beam) can be represented as

$$K_f = \frac{1}{2}\left(\mathcal{M}_f V_0^{aT} V_0^a - 2\mathcal{M}_f \Omega_0^a \widetilde{V}_0^a \xi_f + \Omega_0^{aT} I_f \Omega_0^a\right)$$

$$K_w = \frac{1}{2}\int_0^\ell \left(\mathcal{M}_w V_b^{BT} V_b^B - 2\mathcal{M}_w \Omega_b^B \widetilde{V}_b^B \xi_w + \Omega_b^{BT} I_w \Omega_b^B\right)\mathrm{d}x_1 \tag{2}$$

The gravitational potential energy can be written as

$$G_f = \mathcal{M}_f g \boldsymbol{e}_3^T C^{ia}\left(u_0^a + \xi_f\right)$$

$$G_w = \int_0^\ell \mathcal{M}_w g \boldsymbol{e}_3^T C^{ia}\left(u_0^a + \boldsymbol{r}_b^a + u_b^a + C^{aB}\xi_w\right)\mathrm{d}x_1 \tag{3}$$

The strain energy due to elastic deformation of the wing is given by

$$U = \frac{1}{2}\int_0^\ell \begin{Bmatrix}\gamma\\ \kappa\end{Bmatrix}^T [\mathcal{S}] \begin{Bmatrix}\gamma\\ \kappa\end{Bmatrix}\mathrm{d}x_1 \tag{4}$$

where $[\mathcal{S}]$, the stiffness matrix, can be obtained for an arbitrary cross section using variational asymptotic beam sectional analysis.[18]

The variation of the individual energies is required for substitution into the Hamilton's principle. For the kinetic energy,

$$\delta K = \delta V_0^{aT} P_0^a + \delta \Omega_0^{aT} H_0^a + \int_0^\ell \left(\delta V_b^{BT} P_b^B + \delta \Omega_b^{BT} H_b^B\right)\mathrm{d}x_1 \tag{5}$$

where the expressions for P and H have been derived in Ref. 19 and are given by

$$P = \left(\frac{\partial K}{\partial V}\right)^T = \mathcal{M}(V - \tilde{\xi}\Omega), \qquad H = \left(\frac{\partial K}{\partial \Omega}\right)^T = I\Omega + \mathcal{M}\tilde{\xi}V \tag{6}$$

Similarly, the variation of the potential energy is given by

$$\delta U = \delta G + \int_0^\ell \left(\delta\gamma^T F_b^B + \delta\kappa^T M_b^B\right)\mathrm{d}x_1 \tag{7}$$

where the expressions for F and M are obtained as

$$\begin{Bmatrix}F\\ M\end{Bmatrix} = \begin{Bmatrix}\dfrac{\partial U}{\partial \gamma}^T\\ \dfrac{\partial U}{\partial \kappa}^T\end{Bmatrix} = [\mathcal{S}]\begin{Bmatrix}\gamma\\ \kappa\end{Bmatrix} \tag{8}$$

The virtual work done on the system can be written in terms of the external forces as

$$\overline{\delta W} = \delta u_0^{aT} f_0^a + \overline{\delta\psi}_0^{aT} m_0^a + \int_0^\ell \left(\delta u_b^{aT} f_b^a + \overline{\delta\psi}_b^{aT} m_b^a\right)\mathrm{d}x_1 \tag{9}$$

By the use of the kinematic relationships derived in Ref. 13 and the transformed representation presented in Ref. 19, the expressions for the velocities and the generalized strains can be written as

$$V_0^a = \dot{u}_0^a, \qquad \tilde{\Omega}_0^a = -\dot{C}^{ai}C^{aiT}$$

$$V_b^B = C^{Ba}\left[V_0^a + \tilde{\Omega}_0^a\left(r_b^a + u_b^a\right) + \dot{u}_b^a\right]$$

$$\tilde{\Omega}_b^B = -\dot{C}^{Ba}C^{BaT} + C^{Ba}\tilde{\Omega}_0^a C^{BaT}$$

$$\gamma = C^{Ba}\left(C^{ab}\boldsymbol{e}_1 + u_b^{a\prime}\right) - \boldsymbol{e}_1, \qquad \tilde{\kappa} = (C^{bB}C^{Ba\prime} - C^{ba\prime})C^{ab} \tag{10}$$

Before proceeding any further, it is necessary to define rotational variables to represent the orientation of the aircraft and wing sections. The orientation of B frame with respect to a frame can be represented in terms of Rodrigues parameters. Rodrigues parameters have been applied to nonlinear beam problems with success. Using the Rodrigues parameters, the expressions for the angular velocities and moment strain can be simplified as

$$\Omega_b^B = C^{ba}\left[\frac{\Delta - \left(\tilde{\theta}_b^a/2\right)}{1 + \left(\theta_b^{aT}\theta_b^a/4\right)}\right]\dot{\theta}_b^a + C^{Ba}\Omega_0^a$$

$$\kappa = C^{ba}\left[\frac{\Delta - \left(\tilde{\theta}_b^a/2\right)}{1 + \left(\theta_b^{aT}\theta_b^a/4\right)}\right]\theta_b^{a\prime} \tag{11}$$

For the orientation of the aircraft, that is, of the a frame, the regular use of the Rodrigues parameters is insufficient because of a singularity at rotation of 180 deg. Thus, the direction cosines of a in i will be used as rotational variables. The expression for the angular velocity will automatically constrain the six additional unknowns.

The variational forms of all of the energies and the expressions for all of the variables used therein have been given. In the mixed formulation, the expressions of the variables are enforced as constraints using Lagrange multipliers. By denoting of the expressions of all of the variables by $(\,)^*$, Hamilton's equation becomes

$$\begin{aligned}\int_{t_1}^{t_2} \Bigg\{ &\delta V_0^{a*T} P_0^a + \delta\Omega_0^{a*T} H_0^a + \delta u_0^{aT} f_0^a + \overline{\delta\psi}_0^{aT} m_0^a\\ &- \delta G - \delta V_0^{aT}\left(P_0^a - P_0^{a*}\right) - \delta\Omega_0^{aT}\left(H_0^a - H_0^{a*}\right)\\ &- \delta P_0^{aT}\left(V_0^a - V_0^{a*}\right) - \delta H_0^{aT}\left(\Omega_0^a - \Omega_0^{a*}\right)\\ &+ \int_0^\ell \Big[\delta V_b^{B*T} P_b^B + \delta\Omega_b^{B*T} H_b^B - \delta\gamma^{*T} F_b^B - \delta\kappa^{*T} M_b^B\\ &+ \delta u_b^{aT} f_b^a + \overline{\delta\psi}_b^{aT} m_b^a + \delta\gamma^T\left(F_b^B - F_b^{B*}\right)\\ &+ \delta\kappa^T\left(M_b^B - M_b^{B*}\right) - \delta V_b^{BT}\left(P_b^B - P_b^{B*}\right)\\ &- \delta\Omega_b^{BT}\left(H_b^B - H_b^{B*}\right) + \delta F_b^{BT}(\gamma - \gamma^*)\\ &+ \delta M_b^{BT}(\kappa - \kappa^*) - \delta P_b^{BT}\left(V_b^B - V_b^{B*}\right)\\ &- \delta H_b^{BT}\left(\Omega_b^B - \Omega_b^{B*}\right)\Big]\mathrm{d}x_1\Bigg\}\mathrm{d}t = \overline{\delta\mathcal{A}}\end{aligned} \tag{12}$$

The expressions for various quantities and their variations can be substituted in the preceding equations to get a complete form of Hamilton's equation.

The external forces and moments in the preceding expressions are the various loads acting on the aircraft, including aerodynamic and propulsive loads. Propulsive loads will be treated as given.

Aerodynamic Theory

To have a state-space representation of the aerodynamic problem with a low number of states, the finite state aerodynamic theory of Peters and Johnson[14] is a natural choice. It accounts for large frame (airfoil) motion as well as small deformation of the airfoil in this frame, for example, trailing-edge flap deflection. The theory has been extended to include compressibility effects[15] and gives good dynamic stall results when complemented with the ONERA stall model.[14]

The aerodynamic loads used are as described in detail by Peters and Johnson.[14] The integro–differential airloads equations are converted into ordinary differential equations (ODEs) through a Glauert expansion. The ODEs are in terms of the expansion coefficients, which are represented by a subscript n, so that

$$(1/2\pi\rho)\{L_n\} = -b^2[M]\{\ddot{h}_n + \dot{v}_n\} - bu_0[C]\{\dot{h}_n + v_n - \lambda_0\} - u_0^2[K]\{h_n\} - b[G]\{\dot{u}_0 h_n - u_0 v_n + u_0\lambda_0\}$$

$$(1/2\pi\rho)\{D\} = -b\{\dot{h}_n + v_n - \lambda_0\}^T[S]\{\dot{h}_n + v_n - \lambda_0\} + b\{\ddot{h}_n + \dot{v}_n\}^T[G]\{h_n\} - u_0\{\dot{h}_n + v_n - \lambda_0\}^T[K - H]\{h_n\} + \{\dot{u}_0 h_n - u_0 v_n + u_0\lambda_0\}^T[H]\{h_n\} \tag{13}$$

where $[K]$, $[C]$, $[G]$, $[S]$, $[H]$, and $[M]$ are constant matrices, expressions for which are given in Ref. 14.

The required airloads, namely, lift, moment about midchord, and hinge moment, are obtained as a linear combination of L_n. The theory described so far is basically a linear, thin-airfoil theory. However, the theory lends itself to corrections and modifications from experimental data. Thus, corrections such as thickness and Mach number can be incorporated very easily, as described in Ref. 15. The induced flow λ_0 in Eq. (13) is calculated using the induced-flow model as described next.

Induced-Flow Theory

The induced flow is obtained through the finite state theory of Peters et al.[20] The induced-flow velocity λ_0 is represented in terms of N states, $\lambda_1, \lambda_2, \ldots, \lambda_N$, so that

$$\lambda_0 \approx \frac{1}{2}\sum_{n=1}^{N} b_n\lambda_n \tag{14}$$

where the b_n are found by least-squares method and the λ_n are obtained by solving a set of N first-order differential equations[20] given by

$$\dot{\lambda}_0 - \tfrac{1}{2}\dot{\lambda}_2 + (u_T/b)\lambda_1 = 2\dot{\bar{\Gamma}}$$

$$(1/2n)(\dot{\lambda}_{n-1} - \dot{\lambda}_{n+1}) + (u_T/b)\lambda_n = (2/n)\dot{\bar{\Gamma}} \qquad n \geq 2 \tag{15}$$

where $\bar{\Gamma}$ is the normalized circulation $\Gamma/2\pi b$. The expression for the normalized circulation is calculated based on the deformable airfoil model as

$$\bar{\Gamma} = \{1\}^T[C - G]\{h_n + v_n - \lambda_1\} + (u_0/b)\{1\}^T[K]\{h_n\} \tag{16}$$

Stall Model

The airloads and induced-flow models can be modified to include the effects of dynamic stall according to the ONERA approach. The stall-corrected generalized airloads can be written as

$$L_{T_n} = L_n + \rho u_T\Gamma_n, \qquad n \geq 1$$

$$\Gamma_T = \Gamma + \Gamma_\ell \tag{17}$$

where

$$u_T = \sqrt{u_0^2 + (v_0 + \dot{h}_0 - \lambda_0)^2}$$

$$\ddot{\Gamma}_n + \frac{u_T}{b}\eta\dot{\Gamma}_n + \left(\frac{u_T}{b}\right)^2\omega^2\Gamma_n = -\frac{\omega^2 u_T^3\Delta c_n}{b} - \omega^2 e u_T\frac{\mathrm{d}}{\mathrm{d}t}(u_T\Delta c_n) \tag{18}$$

and the parameters Δc_n, η, ω^2, and e must be identified for a particular airfoil. Γ_ℓ is the correction to the circulation obtained for Δc_ℓ. To calculate the correction to lift $-L_0$ and drag D, the following equations are used, which also include the effect of skin-friction drag:

$$L_{T_0} = L_0 - \rho u_0\Gamma_\ell - c_d u_T(v_0 + \dot{h}_0 - \lambda_0)\rho b$$

$$D_T = D - \rho(v_0 + \dot{h}_0 - \lambda_0)\Gamma_\ell + c_d u_T u_0\rho b \tag{19}$$

The airloads are inserted into Hamilton's principle to complete the aeroelastic model.

Solution of the Aeroelastic System

Coupling the structural and aerodynamics models, one gets the complete aeroelastic model. By selecting the shape functions for the variational quantities in the formulation, one can choose between 1) finite elements in space leading to a set of ordinary nonlinear differential equations in time and 2) finite elements in space and time leading to a set of nonlinear algebraic equations. Using finite elements in space, one can obtain the steady-state solution and calculate linearized equations of motion about the steady state for stability analysis. This state-space representation can also be used for control synthesis. Finite elements in space and time are used to march in time and get the dynamic nonlinear behavior of the system. This kind of analysis is useful in finding the amplitudes of the limit-cycle oscillations and investigating the nonlinear response of the system.

Thus, three kinds of solutions are possible: 1) nonlinear steady-state solution, 2) stability analysis of small motions about the steady state (by linearizing about the steady state), and 3) time-marching solution for nonlinear dynamics of the system.

For steady-state and stability analysis, the formulation is converted to it weakest form in space, while retaining the time derivatives of variables. This is achieved by transferring the spatial derivatives of variables to the corresponding variation by integration by parts. Because of the formulation's weakest form, simplest shape functions can be used.[13] With these shape functions, the spatial integration in Eq. (12) can be performed explicitly to give a set of nonlinear equations.[16] These equations can be separated into structural, F_S, and aerodynamic, F_L, terms and written as

$$F_S(X, \dot{X}) - F_L(X, Y, \dot{X}) = 0 \tag{20}$$

Similarly, one can separate the induced-flow equations into an induced-flow component F_I and a downwash component F_W as

$$-F_W(\dot{X}) + F_I(Y, \dot{Y}) = 0 \tag{21}$$

The solutions of interest for the two coupled sets of equations [Eqs. (20) and (21)] can be expressed in the form

$$\begin{Bmatrix} X \\ Y \end{Bmatrix} = \begin{Bmatrix} \bar{X} \\ \bar{Y} \end{Bmatrix} + \begin{Bmatrix} \hat{X}(t) \\ \hat{Y}(t) \end{Bmatrix} \tag{22}$$

For the steady-state solution, one gets $\bar{Y}$ identically equal to zero [from Eq. (21)]. Thus, one has to solve a set of nonlinear equations given by

$$F_S(\bar{X}, 0) - F_L(\bar{X}, 0, 0) = 0 \tag{23}$$

The Jacobian matrix of the preceding set of nonlinear equations can be obtained analytically and is found to be very sparse.[16] The steady-state solution can be found very efficiently using the Newton–Raphson method.

By the perturbing of Eqs. (20) and (21) about the calculated steady state using Eq. (22), the transient solution is obtained from

$$\begin{bmatrix} \frac{\partial F_S}{\partial \dot{X}} - \frac{\partial F_L}{\partial \dot{X}} & 0 \\ -\frac{\partial F_W}{\partial \dot{X}} & \frac{\partial F_I}{\partial \dot{Y}} \end{bmatrix}_{\substack{X=\bar{X} \\ Y=0}} \begin{Bmatrix} \dot{\hat{X}} \\ \dot{\hat{Y}} \end{Bmatrix}$$

$$+ \begin{bmatrix} \frac{\partial F_S}{\partial X} - \frac{\partial F_L}{\partial X} & -\frac{\partial F_L}{\partial Y} \\ 0 & \frac{\partial F_I}{\partial Y} \end{bmatrix}_{\substack{X=\bar{X} \\ Y=0}} \begin{Bmatrix} \hat{X} \\ \hat{Y} \end{Bmatrix} = \begin{Bmatrix} 0 \\ 0 \end{Bmatrix} \tag{24}$$

By assuming that the dynamic modes are of the form e^{st} the preceding equations can be solved as an eigenvalue problem to get the modal damping, frequency, and mode shape of the various modes. The stability condition of the aeroelastic system at various operating conditions is, thus, obtained.

To investigate the nonlinear dynamics of the aircraft, a time history of aircraft motion has to be obtained. To get such a solution, space–time finite elements are used. This requires that the formulation be converted into its weakest form in space as well as time. Thus, the spatial and temporal derivatives are transferred to the variations. Again because of the weakest form of the variational statement, constant shape functions are used for the variables, and linear/bilinear shape functions are used for the test functions.[21] With these shape functions, Eqs. (20) and (21) take the form

$$F_S(X_i, X_f) - F_L(X_i, X_f, Y) = 0$$

$$-F_W(X_i, X_f) + F_I(Y_i, Y_f) = 0 \tag{25}$$

where subscripts i and f are the variable values at the initial and final time. If the initial conditions and time interval are specified, the variable values at the final condition are obtained by solving the set of nonlinear equations.

Numerical Results

Flutter and divergence results have been obtained for a metallic wing model presented by Goland.[22] Linear results are compared with published results. The linear and nonlinear results obtained indicate that the steady-state solution and the eigenvalues can be computed efficiently and are accurate. The time-marching scheme based on space–time finite elements was found to be stable. Aeroelastic tailoring of a composite box beam wing was conducted in earlier papers[6,7] and will not be repeated here.

The Goland wing data[22] is reproduced in Table 1. The results are shown in Table 2. The current analysis gives the flutter speed and flutter frequency results to within 1% of the exact linear flutter speed of the cantilevered wing.

The lift-curve slope and stall data for the airfoil are obtained by curve fitting the empirical c_ℓ and c_m. Figure 1 shows the assumed linear and stall data for the results presented. The coefficients for the dynamic stall model, that is, η, ω, and e, as functions of Δc_ℓ are assumed for the present symmetric airfoil to be[23]

$$\eta = 0.25 + 0.10(\Delta c_\ell)^2, \qquad \omega = 0.20 + 0.10(\Delta c_\ell)^2$$

$$e = 3.3 - 0.3(\Delta c_\ell)^2 \tag{26}$$

Table 1 Goland[22] wing structural data

Property	Value
Wing half span	20 ft
Wing chord	6 ft
Mass per unit length	0.746 slugs/ft
Radius of gyration of wing about mass center	25% of chord
Spanwise elastic axis of wing	33% of chord (from leading edge)
Center of gravity of wing	43% of chord (from leading edge)
Bending rigidity, EI_b	23.65×10^6 lb ft^2
Torsional rigidity, GJ	2.39×10^6 lb ft^2

Effect of Nonlinearities on Flutter

Structural as well as aerodynamic nonlinearities are known to affect flutter. One of the goals of this research is to be able to determine up front those cases for which nonlinear models are essential for accuracy. As a first step toward that goal, flutter analysis is conducted on the Goland[22] cantilevered wing. The gravitational forces and skin-friction drag are neglected in these results. Figure 2 shows the variation of the flutter speed with increasing angle of attack. The results show the effect of structural nonlinearities and dynamic stall nonlinearities on the flutter speed.

As the angle of attack is increased, the aerodynamic load on the wing increases and so do the bending and torsional displacements. The flutter speed is seen to increase due to geometric stiffening. The results including dynamic stall model are markedly different from those without. This is due to coupling between the structural states and the stall states. The stall delay frequency of around 25 rad/s interacts with the first two structural modes and leads to additional coupling and coalescence and, thus, change in flutter mode. The flutter mode frequency shifts from around 70 rad/s at 7 deg to 55 rad/s at 12 deg. Also as the angle of attack is increased, wing stall occurs at lower speeds, thus leading to possibility of flutter at lower speeds.

The effects of structural nonlinearities seem to be small in the preceding test case, which is a relatively low-aspect-ratio conventional wing. Potentially, however, the effects would be considerably higher for a flexible high-aspect-ratio wings used in UAVs.[24]

Table 2 Comparison of flutter results for Goland[22] wing

Method	Flutter velocity, ft/s	Flutter frequency, rad/s
Present analysis	445	70.2
Exact solution	450	70.7
Galerkin solution	445	70.7

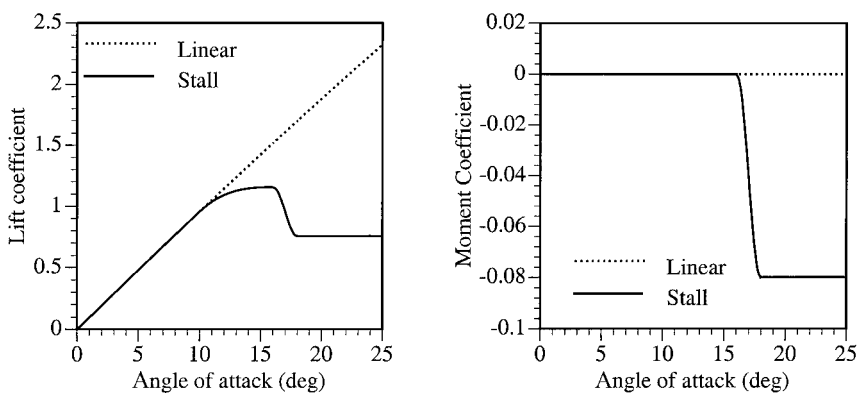

Fig. 1 Linear and stall data for c_ℓ and c_m.

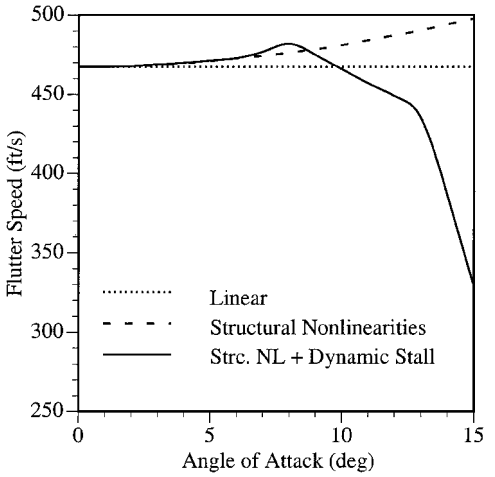

Fig. 2 Variation of flutter speed with angle of attack.

Limit-Cycle Oscillations

The flutter results obtained in the earlier section give the velocity of onset of flutter. These flutter results imply that small disturbances will grow exponentially for velocities higher than the flutter speed. However, as the amplitude of oscillations grows, so does the additional nonlinear stiffness. Consequently, the vibrations do not grow to infinity, but instead converge to a limit-cycle oscillation (LCO). The amplitude of the LCO gives an idea of the amount of stress/strain on the structure and, thus, is useful in failure analysis and design. The amplitude, phase, and type of LCO can be determined by time marching the nonlinear differential equations of motion of the aeroelastic system.

The Goland[22] wing at zero steady-state angle of attack and a velocity of 500 ft/s ($V_F = 468$ ft/s) was disturbed by a small disturbance, and the time history of oscillations was obtained. The tip displacement, tip rotation, and the total energy (sum of kinetic and potential energy) are plotted against time in Fig. 3. The tip displacement and rotation increase exponentially when the amplitude of vibration is small, that is, the nonlinearities are negligible. As the

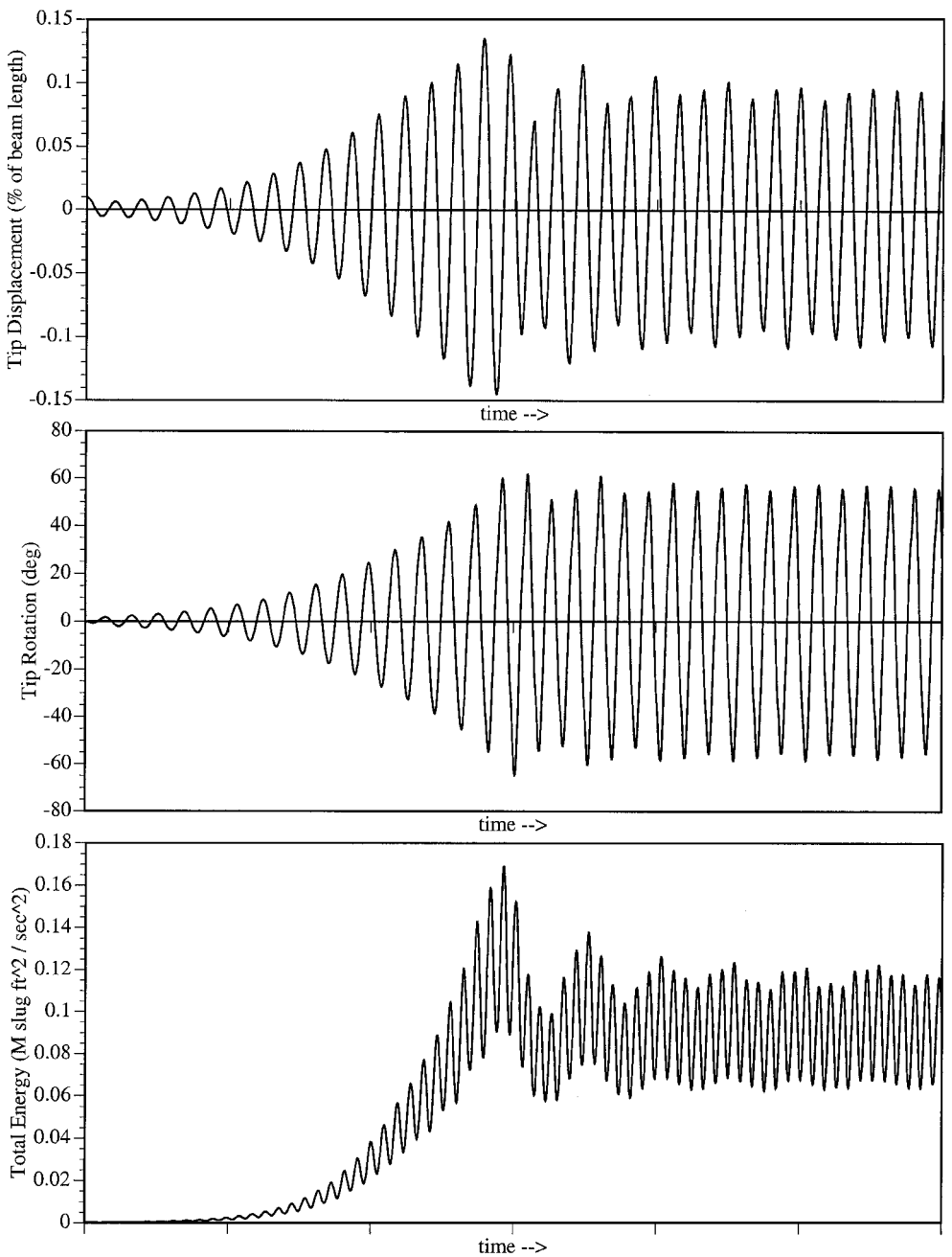

Fig. 3 Time history showing LCO above flutter speed.

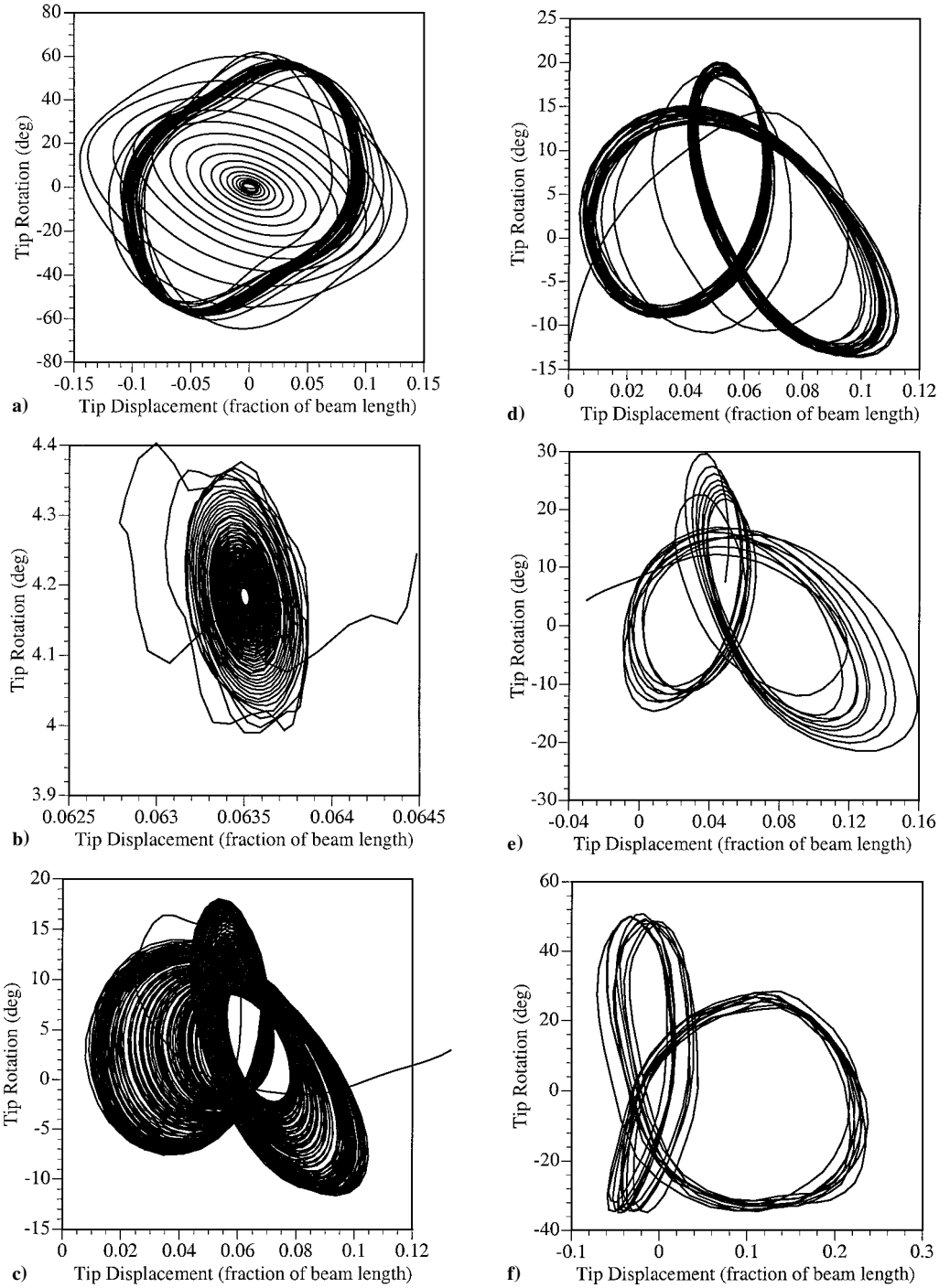

Fig. 4 Phase-plane diagrams for various initial disturbances.

amplitude of vibration increases, nonlinearities due to stall become important and in fact dominant. The aerodynamic forcing function drops and, thus, can no longer pump the required amount of energy into the structure, and the amplitude of oscillation and the total energy levels out.

Another way of looking at the history of oscillations is via a phase plane plot. Here two variables of the system are plotted against each other to give an insight into the mode shape of oscillation. Figure 4 shows the plot of tip displacement vs tip rotation. One can clearly see the changes in the mode shape as the amplitude increases and eventually settles into a LCO.

Effect of Large Disturbances

Stability as calculated by eigenvalues is a linear concept and, thus, is valid for small disturbances about the steady state. The flutter speeds calculated earlier predict that small disturbances grow for speeds higher than the flutter speed and decay for lower speeds. However, the disturbances encountered by an aircraft depend completely on its mission and environment, for example, maneuvers and gust amplitudes. A nonlinear system found to be stable under small disturbances may not necessarily maintain stability for higher amplitudes of disturbances. In fact, the dynamics of the system can be completely different for varying initial conditions.

Consider the Goland[22] wing at 10-deg steady-state angle of attack flying with a velocity of 450 ft/s ($V_F = 466$ ft/s). Figure 5 shows the response of the system for various initial conditions. The initial conditions are obtained by deforming the wing with tip forces and moments. S denotes a stable response, L denotes a mode that is either an LCO or very lightly damped oscillation, and U denotes that the initial mode shape is unstable and, thus, the amplitude of oscillation increases and finally settles into a new higher amplitude

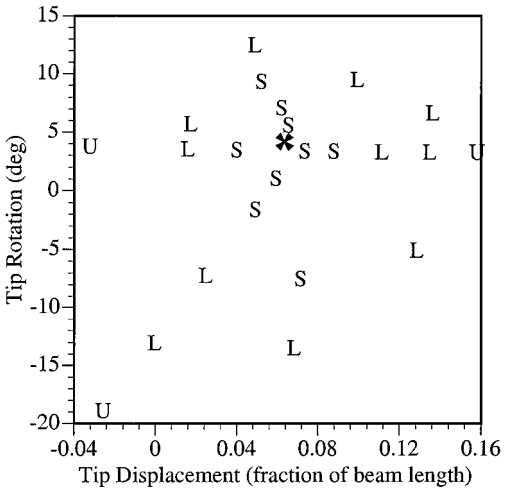

Fig. 5 Stability at various initial conditions.

LCO. The reason to distinguish between the latter two responses is that the first one has a small amplitude and most likely will not result in structural failure. Figure 5 shows that, depending on the disturbance, the wing may go into a flutter/LCO even at speeds lower than the flutter speed.

The mode shapes represented in the phase plane are given in Fig. 4. Figure 4b shows the behavior of the system for small disturbances. It is lightly damped and the mode shape is that obtained by a linear eigenvalue solution. Figures 4c and 4d show the kind of responses for medium-level disturbances. The mode shape is nonlinear, that is, nonsinusoidal, and depending on the disturbance the damping is either zero or very close to it (Fig. 4d) or small (Fig. 4c). Figures 4e and 4f show the initial and final mode shape for high-power disturbance. Two plots have been made for easier visualization. Figure 4e clearly shows that the amplitude of vibration is increasing, and Fig. 4f shows the final converged large-amplitude LCO.

Conclusions

A theoretical basis for nonlinear aeroelastic analysis of aircraft in subsonic flow has been presented. It takes into account structural geometric nonlinearities and aerodynamic stall nonlinearities. The equations for the aeroelastic system have been solved using low-order finite elements. Examples of different nonlinear aeroelastic effects have been presented.

Although the results presented are somewhat complex, they still provide insight into the effects of nonlinearities on aeroelastic stability. Structural nonlinearities were stiffening for the wing considered. Stall nonlinearities decreased the flutter speeds drastically due to coupling between the low-frequency stall dynamics and structural modes. LCOs were observed, but the amplitude was very high, which might lead to failure in an actual wing. A very interesting nonlinear effect was that of finite disturbances. It has been shown that even for speeds lower than the predicted linearized instability speed, instabilities could be induced due to finite disturbances.

Acknowledgments

This work was supported by the U.S. Air Force Office of Scientific Research (Grant F49620-98-1-0032), Brian P. Sanders, Technical Monitor. Technical discussions with David A. Peters are gratefully acknowledged.

References

[1]Patil, M. J., Hodges, D. H., and Cesnik, C. E. S., "Nonlinear Aeroelastic Analysis of Aircraft with High-Aspect-Ratio Wings," *Proceedings of the 39th Structures, Structural Dynamics, and Materials Conference*, AIAA, Reston, VA, 1998, pp. 2056–2068.

[2]Shirk, M. H., Hertz, T. J., and Weisshaar, T. A., "Aeroelastic Tailoring: Theory, Practice, and Promise," *Journal of Aircraft*, Vol. 23, No. 1, 1986, pp. 6–18.

[3]Librescu, L., and Song, O., "On the Static Aeroelastic Tailoring of Composite Aircraft Swept Wings Modelled as Thin-Walled Beam Structures," *Composites Engineering*, Vol. 2, No. 5–7, 1992, pp. 497–512.

[4]Butler, R., and Banerjee, J. R., "Optimum Design of Bending–Torsion Coupled Beams with Frequency or Aeroelastic Constraints," *Computers and Structures*, Vol. 60, No. 5, 1996, pp. 715–724.

[5]Chattopadhyay, A., Zhang, S., and Jha, R., "Structural and Aeroelastic Analysis of Composite Wing Box Sections Using Higher-Order Laminate Theory," *Proceedings of the 37th Structures, Structural Dynamics, and Materials Conference*, AIAA, Reston, VA, 1996, pp. 2185–2198.

[6]Cesnik, C. E. S., Hodges, D. H., and Patil, M. J., "Aeroelastic Analysis of Composite Wings," *Proceedings of the 37th Structures, Structural Dynamics, and Materials Conference*, AIAA, Reston, VA, 1996, pp. 1113–1123.

[7]Patil, M. J., "Aeroelastic Tailoring of Composite Box Beams," AIAA Paper 97-0015, 1997.

[8]van Schoor, M. C., and von Flotow, A. H., "Aeroelastic Characteristics of a Highly Flexible Aircraft," *Journal of Aircraft*, Vol. 27, No. 10, 1990, pp. 901–908.

[9]Waszak, M. R., and Schmidt, D. K., "Flight Dynamics of Aeroelastic Vehicles," *Journal of Aircraft*, Vol. 25, No. 6, 1988, pp. 563–571.

[10]Dunn, P., and Dugundji, J., "Nonlinear Stall Flutter and Divergence Analysis of Cantilevered Graphite/Epoxy Wings," *AIAA Journal*, Vol. 30, No. 1, 1992, pp. 153–162.

[11]Virgin, L. N., and Dowell, E. H., "Nonlinear Aeroelasticity and Chaos," *Computational Nonlinear Mechanics in Aerospace Engineering*, edited by S. N. Atluri, AIAA, Washington, DC, 1992, Chap. 15.

[12]Gilliatt, H. C., Strganac, T. W., and Kurdila, A. J., "Nonlinear Aeroelastic Response of an Airfoil," AIAA Paper 97-0459, 1997.

[13]Hodges, D. H., "A Mixed Variational Formulation Based on Exact Intrinsic Equations for Dynamics of Moving Beams," *International Journal of Solids and Structures*, Vol. 26, No. 11, 1990, pp. 1253–1273.

[14]Peters, D. A., and Johnson, M. J., "Finite-State Airloads for Deformable Airfoils on Fixed and Rotating Wings," *Proceedings of the Winter Annual Meeting*, Vol. 44, American Society of Mechanical Engineers, Nov. 1994, pp. 1–28.

[15]Peters, D. A., Barwey, D., and Johnson, M. J., "Finite-State Airloads Modeling with Compressibility and Unsteady Free-Stream," *Proceedings of the Sixth International Workshop on Dynamics and Aeroelastic Stability Modeling of Rotorcraft Systems*, U.S. Army Research Office, Los Angeles, 1995.

[16]Hodges, D. H., Shang, X., and Cesnik, C. E. S., "Finite Element Solution of Nonlinear Intrinsic Equations for Curved Composite Beams," *Journal of the American Helicopter Society*, Vol. 41, No. 4, 1996, pp. 313–321.

[17]Hodges, D. H., Atilgan, A. R., Cesnik, C. E. S., and Fulton, M. V., "On a Simplified Strain Energy Function for Geometrically Nonlinear Behaviour of Anisotropic Beams," *Composites Engineering*, Vol. 2, No. 5–7, 1992, pp. 513–526.

[18]Cesnik, C. E. S., and Hodges, D. H., "VABS: A New Concept for Composite Rotor Blade Cross-Sectional Modeling," *Journal of the American Helicopter Society*, Vol. 42, No. 1, 1997, pp. 27–38.

[19]Shang, X., and Hodges, D. H., "Aeroelastic Stability of Composite Rotor Blades in Hover," *Proceedings of the 36th Structures, Structural Dynamics, and Materials Conference*, AIAA, Washington, DC, 1995, pp. 2602–2610.

[20]Peters, D. A., Karunamoorthy, S., and Cao, W.-M., "Finite State Induced Flow Models, Part I: Two-Dimensional Thin Airfoil," *Journal of Aircraft*, Vol. 32, No. 2, 1995, pp. 313–322.

[21]Atilgan, A. R., Hodges, D. H., Ozbek, A. M., and Zhou, W., "Space–Time Mixed Finite Elements for Rods," *Journal of Sound and Vibration*, Vol. 192, No. 3, 1996, pp. 731–739.

[22]Goland, M., "The Flutter of a Uniform Cantilever Wing," *Journal of Applied Mechanics*, Vol. 12, No. 4, 1945, pp. A197–A208.

[23]Peters, D. A., Barwey, D., and Su, A., "An Integrated Airloads-Inflow Model for Use in Rotor Aeroelasticity and Control Analysis," *Mathematical and Computational Modelling*, Vol. 19, No. 3/4, 1994, pp. 109–123.

[24]Patil, M. J., Hodges, D. H., and Cesnik, C. E. S., "Nonlinear Aeroelasticity and Flight Dynamics of High-Altitude Long-Endurance Aircraft," *Proceedings of the 40th Structures, Structural Dynamics, and Materials Conference*, AIAA, Reston, VA, 1999, pp. 2224–2232.